Journal of Electronic Materials (2022) 51:838–846
https://doi.org/10.1007/s11664-021-09363-z

ORIGINAL RESEARCH ARTICLE

Polarization-Engineered p-Type Electron-Blocking-Layer-Free III-Nitride Deep-Ultraviolet Light-Emitting Diodes for Enhanced Carrier Transport

Ravi Teja Velpula[1] · Barsha Jain[1] · Trupti Ranjan Lenka[2] · Renjie Wang[3] · Hieu Pham Trung Nguyen[1]

Received: 12 September 2021 / Accepted: 22 November 2021 / Published online: 3 January 2022

Abstract

Electron leakage is one of the critical challenges in AlGaN ultraviolet (UV) light-emitting diodes (LEDs). In this regard, a *p*-type AlGaN electron-blocking layer (EBL) has been utilized to suppress electron leakage. However, it affects the hole injection due to the generation of positive polarization sheet charges at the hetero-interface of the EBL and the last quantum barrier (QB). To address this problem, we propose an EBL-free AlGaN UV LED using polarization-engineered graded QBs instead of conventional QBs. The proposed structure could enhance the carrier confinement in the active region and significantly reduces electron leakage due to the progressively increased effective conduction band barrier heights. Substantially, the proposed structure exhibits higher optical power and wall-plug efficiency at 60 mA current injection, which are boosted by ~85.9% and ~53.6% compared to the conventional structure. Such a unique LED design could pave the way for the next generation of high-power deep UV light sources.

Keywords Ultraviolet light-emitting diodes · AlGaN · electron-blocking layer · polarization sheet charge · wall-plug efficiency

Introduction

Wide bandgap semiconductor light emitters, which are non-toxic, compact, and flexible for many applications, exhibit tremendous potential over the traditional bulky and toxic mercury ultraviolet (UV) lamps.[1] The III-nitride materials such as AlInN and AlGaN are uniquely suited for many applications as the alloys are direct bandgap semiconductors in the entire UV regime.[2,3] To date, research related to AlInN UV light-emitting diodes (LEDs) is still in the infant stage,[4,5] whereas AlGaN UV LEDs have been studied extensively.[6,7] However, the external quantum efficiency (EQE) and light output power of the AlGaN deep-UV LEDs are still impoverished compared to their visible counterparts.[6,8] Induced polarization fields causing low carrier confinement and electron overflow are two of the critical challenges for poor efficiency. To improve the carrier confinement and suppress the electron leakage to the *p*-region, an Al-rich *p*-type electron-blocking layer (EBL) is introduced just after the active region.[9] This could alleviate the electron leakage up to an extent. However, at the last quantum barrier (QB) and EBL interface, a positive polarization sheet charge region may be created. It is found that electrons are accumulating and contributing to non-radiative recombination in this region.[10] Moreover, due to this positive polarization sheet charge, hole injection efficiency is also reduced.[11,12] The Mg acceptor activation energy of the Al-rich EBL layer is elevated and further affects the Mg doping efficiency. To overcome the problems due to the incorporation of a conventional EBL, the EBL is re-designed using a graded layer,[13] superlattice layers,[14] and graded superlattice layers.[12,15] Using these approaches, challenges related to the EBL are partially mitigated. However, it is always desired to develop EBL-free UV LEDs for better carrier transport and overcome the aforementioned challenges related to the

✉ Hieu Pham Trung Nguyen
hieu.p.nguyen@njit.edu

[1] Department of Electrical and Computer Engineering, New Jersey Institute of Technology, Newark, NJ 07102, USA

[2] Department of Electronics and Communication Engineering, National Institute of Technology Silchar, Assam 788010, India

[3] Department of Electrical and Computer Engineering, University of Virginia, Charlottesville, VA 22904, USA

EBL. Here, we have introduced a p-type EBL-free AlGaN deep UV LED structure with linearly graded polarization-controlled QBs instead of conventional QBs in the active region, where the height of each QB is increasing progressively. This design could reduce the electrostatic field in the quantum well (QW) region because of the reduced lattice mismatch between the QW and the QB. In addition, due to a progressive increase in the effective conduction band barrier heights (CBBHs), the proposed structure improves the carrier confinement in the active region and reduces the electron leakage to the *p*-region.[16] Moreover, the formation of positive polarization sheet charges at the last QB and EBL interface is negligible due to the elimination of EBL that improves the hole injection efficiency significantly. Consequently, output power and wall-plug efficiency (WPE) of the proposed LED structure are notably enhanced as compared to the conventional LED.

Device Structure and Parameters

In this study, three LED devices were designed and their performance was scrutinized. A conventional AlGaN deep UV LED structure (LED 1) with ~284 nm emission wavelength, reported experimentally by Yan et al.,[17] is considered as a reference structure. As illustrated in Fig. 1a, LED 1 comprises a 3 µm *n*-$Al_{0.6}Ga_{0.4}N$ (Si: 5×10^{18} cm^{-3}) template layer, an active region composed of five intrinsic 3 nm $Al_{0.4}Ga_{0.6}N$ QWs sandwiched between six intrinsic 12-nm-thick $Al_{0.5}Ga_{0.5}N$ QBs, a 20 nm *p*-$Al_{0.65}Ga_{0.35}N$ (Mg: 2×10^{19} cm^{-3}) EBL, a 50 nm *p*-$Al_{0.5}Ga_{0.5}N$ (Mg: 2×10^{19} cm^{-3}) hole injection layer, and a 120 nm *p*-GaN (Mg: 1×10^{20} cm^{-3}) contact layer. Furthermore, the Al composition (%) profile information for LED 1 is shown in Fig. 1b. Importantly, we have precisely validated our simulation model and the parameters by fitting our simulation results of LED 1 with their experimental data. LED 2 was then constructed from LED 1 by removing the EBL and introducing the higher Al composition in the QBs. The Al composition in each QB is 51%, 54%, 57%, 60%, and 75%, respectively, as depicted by Fig. 1c. Finally, the proposed structure (LED 3) that is shown in Fig. 1d is identical to LED 2 except for the QBs, where the QBs were linearly graded from 51%, 54%, 57%, 60%, and 75% to 50%. The chip area of all LEDs is considered as 400×400 μm^2.

The Advanced Physical Models of Semiconductor Devices (APSYS) tool, provided by Crosslight Inc., is utilized to investigate the performance of AlGaN deep UV LED structures. In this work, we have estimated the energy bandgap of AlN and GaN using the Varshni formula[18]

$$E_g(T) = E_g(0) - \frac{\alpha T^2}{\beta + T} \tag{1}$$

Here, α and β are material constants. $E_g(0)$ and $E_g(T)$ are the energy bandgap at temperatures 0 and T K, respectively. The values of α, β, and E_g (0) for AlN are 1.799 meV/K, 1462 K, and 6.23 eV.[18] The corresponding values for GaN are 0.909 meV/K, 830 K, and 3.507 eV, respectively.[18] The energy bandgap of $Al_mGa_{1-m}N$ is calculated using Eq 2, as shown below:

$$E = m \cdot E^{AlN} + (1 - m) \cdot E^{GaN} - b \cdot m \cdot (1 - m) \tag{2}$$

Here, bowing parameter b = 0.94 is considered.[19] The band offset ratio for the III-nitride material hetero-junctions is assumed as 0.67/0.33.[12] The Auger recombination coefficient, radiative recombination coefficient, Shockley-Read-Hall (SRH) recombination coefficient, and light extraction efficiency are taken as 2.88×10^{-30} cm^6/s, 2.13×10^{-11} cm^3/s, 6.67×10^7 /s, and 15%, respectively.[20,21] Also, the Mg activation energy is set to scale linearly from 170 meV to 510

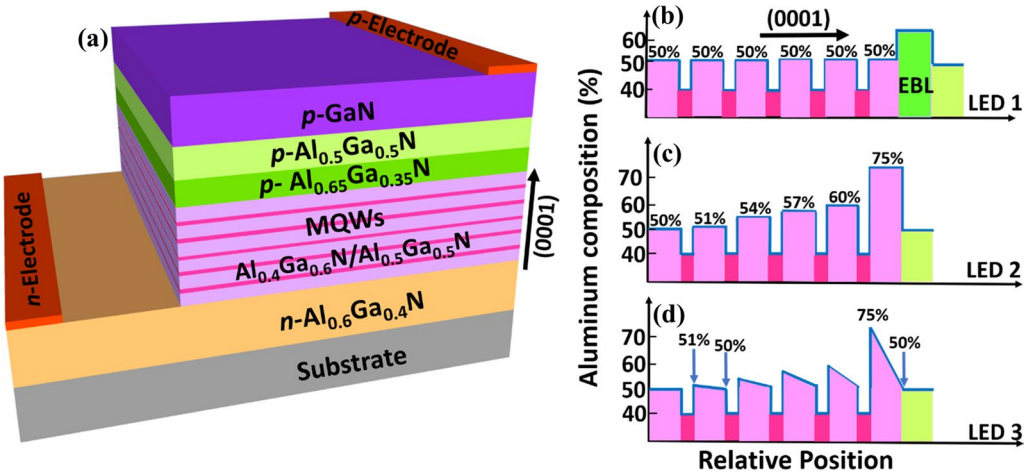

Fig. 1 (a) Schematic diagram of LED 1, Al composition (%) profile related to the conduction band of (b) LED 1, (c) LED 2, and (d) LED 3.

meV for p-$Al_xGa_{(1-x)}N$ alloy where 0<x<1.[22] Further, using the methods proposed by Fiorentini *et al.*, we have estimated the induced polarization due to both piezoelectric and spontaneous polarization[23] and set it as 50% of the theoretical value in our model. By utilizing the 6×6 *k.p* model, energy-band diagrams of all LED structures are calculated,[24] and other band parameters can be found elsewhere.[25]

The simulated and measured[17] light output power-current-voltage (L-I-V) characteristics of our reference structure, LED 1, are presented in Fig. 2a. It is evident that the simulated L-I-V curves closely match the experimentally measured curves, which validates the reliability of our device model and the parameters used in this model. Also, experimental investigations of III-nitride QWs reveal weaker polarization than predicted theoretical values.[26] Therefore, it is required to input an appropriate degree of polarization in our model. To evaluate this value, we have estimated the light output power-current (L-I) characteristics of LED 1 by considering 10%-60% of total polarization values. From Fig. 2b, it is observed that L-I curves with a 50% degree of polarization nearly match experimentally reported values and the same is utilized in our study. With this confirmation, we have further modeled LED 2 and LED 3 structures.

Results and Discussion

To understand the performance of the three deep UV LED structures, we have calculated the energy-band diagrams at an injection current of 60 mA, as shown in Fig. 3. Firstly, the effective CBBHs which is the maximum difference between the conduction band energy level and its quasi-Fermi level for electrons in the corresponding QB (n) and EBL are denoted as ϕ_{en}, and ϕ_{EBL}, respectively. The corresponding values are estimated from the energy-band diagrams and listed in Table I. The ϕ_{EBL} to block the electron overflow in the case of the conventional LED is 235 meV. This value is relatively low compared with the last QB heights (ϕ_{e6}) of LED 2 and LED 3 without EBL. Both LED 2 and LED 3 show a progressive increase in ϕ_{en} values with each QB due to the gradual increment in Al-compositions of QBs, thereby progressively preventing the electrons from jumping out of the QWs. Also, in comparison with LED 3, the ϕ_{en} values are relatively high in LED 2 due to constant barrier compositions. It should generally help in improving the electron confinement in the active region. However, the fact of a very high lattice mismatch between the QBs and QWs in LED 2 leads to generating higher electric fields in the active region that is affecting the carrier confinement and will be explained later in this section. Further, ϕ_{e6} of LED 3 is higher than the ϕ_{EBL} of LED 1 and ϕ_{e6} of LED 2. Thus, it is expected that LED 3 can eminently mitigate the electron leakage from the active region.

Secondly, as illustrated in Fig. 3a, it is worth noting that in the last QB of LED 1, a sharp bending in the conduction band is created due to indued positive polarization sheet charges at the hetero-interface of the EBL and the last QB. A large number of electrons i.e., ~ 3.66×10^{16} cm^{-3}, get accumulated in this region, which eventually contributes to non-radiative recombination.[10] Also, a hole depletion region is formed at the hetero-interface of the EBL and the last QB due to the same positive polarization sheet charges in the valence band of LED 1, as seen from Fig. 3a. This strongly affects the hole injection efficiency into the active region.[11] Whereas, in the case of LED 2 and LED 3, the problem mentioned earlier is eliminated by removing the EBL. Moreover, as shown in Figs. 3b and c, EBL-free LED architectures support the formation of negative sheet polarization charges at the interface of p-$Al_{0.5}Ga_{0.5}N$ and the last QB that boosts the hole injection efficiency.

Lastly, the effective valence band barrier heights (VBBHs), defined as the maximum difference between

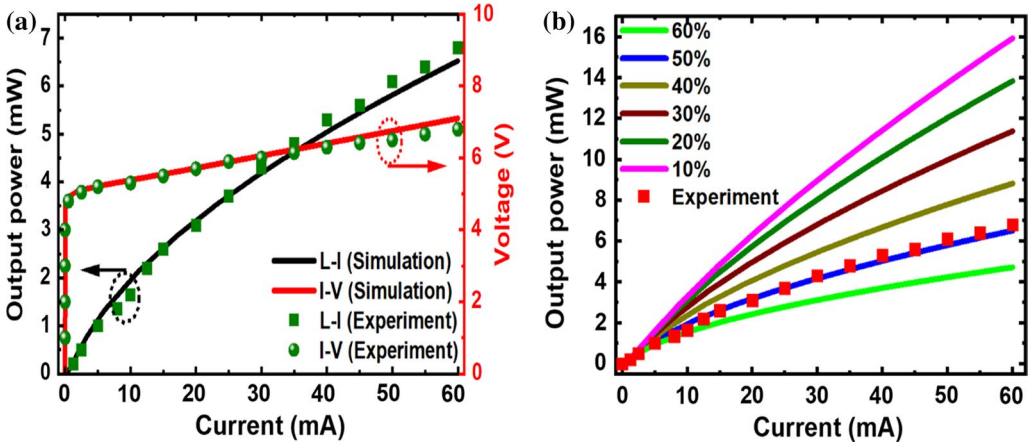

Fig. 2 (a) Simulated and measured L-I-V characteristics of LED 1, (b) L-I characteristics of LED 1 at different degrees of polarization.

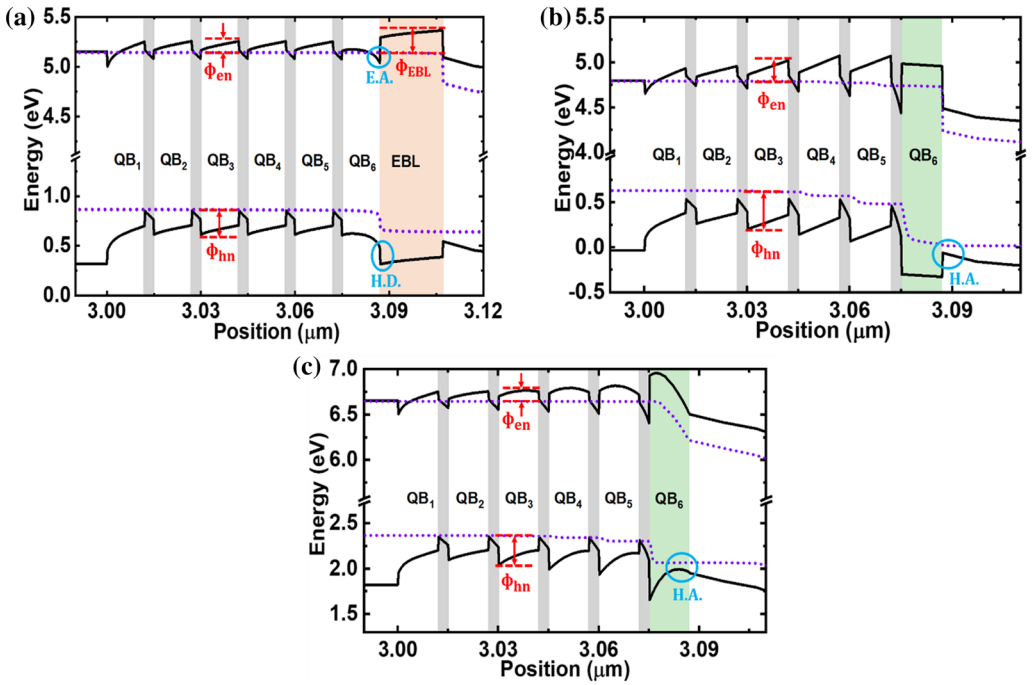

Fig. 3 Estimated energy-band diagrams of (a) LED 1, (b) LED 2, and (c) LED 3 at an injection current of 60 mA. E.A. is the electron accumulation region in the conduction band, H.D. is the hole depletion region, and H.A. is the hole accumulation region in the valence band.

Table I. Effective Conduction Band Barrier Heights of QBs (ϕ_{en}) and EBL (ϕ_{EBL}) for LED 1, LED 2, and LED 3.

CBBH	LED 1	LED 2	LED 3
ϕ_{e1}	107.5 meV	142.9 meV	107.2 meV
ϕ_{e2}	114.3 meV	167.3 meV	109.9 meV
ϕ_{e3}	113.8 meV	232.6 meV	120.0 meV
ϕ_{e4}	112.6 meV	300.6 meV	149.2 meV
ϕ_{e5}	110.1 meV	330.1 meV	175.2 meV
ϕ_{e6}	31.2 meV	242.2 meV	314.7 meV
ϕ_{EBL}	235 meV	–	–

Table II. Effective Valence Band Barrier Heights of QBs (ϕ_{hn}) for LED 1, LED 2 and LED 3.

VBBH	LED1	LED2	LED3
ϕ_{h2}	251.9 meV	367.1 meV	270.8 meV
ϕ_{h3}	250.3 meV	427.1 meV	321.7 meV
ϕ_{h4}	249.3 meV	471.4 meV	367.2 meV
ϕ_{h5}	248.1 meV	502.1 meV	405.9 meV

the valence band energy level and its quasi-Fermi level for holes at the corresponding QB (n) is named as ϕ_{hn}. The corresponding values are calculated and listed in Table II. It is found that the values of ϕ_{hn} are high in LED 2 and LED 3 compared to LED 1 because of an increase in Al composition in the QBs. This supports improving the hole concentration and confinement in the active region. At the same time, a very high ϕ_{hn} can also affect the hole transportation in the active region, which is the case of LED 2. LED 3 has smaller values of ϕ_{hn} as compared to LED 2 due to the graded composition of the QBs. Altogether, it is anticipated that the proposed structure (i.e., LED 3) can demonstrate more efficient hole transportation in the active region compared to other LEDs.

The electron concentration, electron leakage, hole concentration, and radiative recombination of the three LED structures at an injection current of 60 mA are shown in Fig. 4. For better visualization, the position on X-axis is slightly shifted for LEDs. As expected, in comparison with other LEDs, LED 3 shows a relatively improved electron concentration in the active region, as shown in Fig. 4a. Moreover, it is progressively increasing due to the specially designed QBs. Due to the effective confinement of electrons in LED 3, electron leakage into the *p*-region is tremendously reduced compared to the other two LEDs, as presented in Fig. 4b. It is also observed that LED 2 has even larger electron leakage than LED 1 due to the inefficient confinement of electrons in the active region of LED 2. This would increase the non-radiative recombination in the *p*-region for LED 2 and reduces the hole injection efficiency. Although there is a formation of negative sheet polarization charges at the interface of *p*-$Al_{0.5}Ga_{0.5}N$/last QB, hole injection efficiency into the active region is strongly affected due to

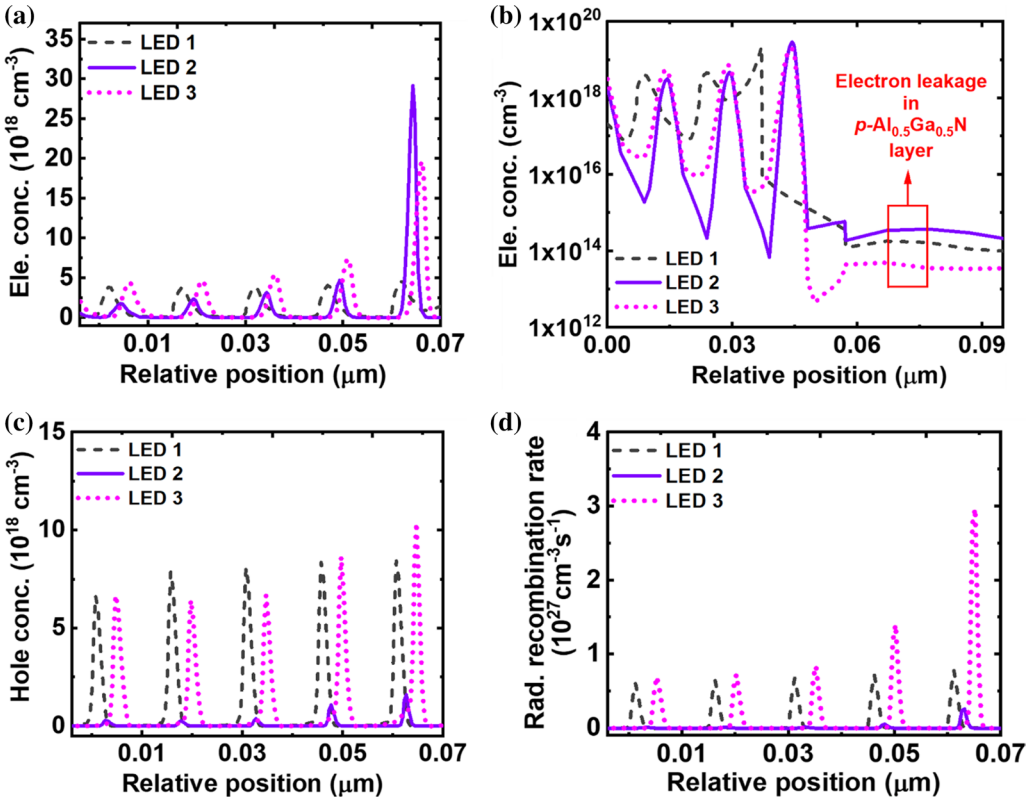

Fig. 4 Calculated (a) Electron concentration, (b) Electron leakage, (c) Hole concentration, and (d) Radiative recombination of LED 1, LED 2, and LED 3.

severe electron leakage in LED 2. Because of the reduced electron leakage in LED 3, the probability of non-radiative recombination of the overflowed electrons with the incoming holes would be reduced in the *p*-region. This would improve the hole injection efficiency to the active region. As a result, LED 3 has enhanced hole concentration and LED 2 has the lowest hole concentration in the active region compared to other LEDs, as depicted in Fig. 4c. Due to improved electron and hole concentrations in LED 3, radiative recombination improved greatly, as illustrated in Fig. 4d. Though the last QB of LED 2 can accommodate higher electrons due to severe band bending but failed to confine the holes; as a result, it exhibits deficient radiative recombination.

To better understand the physical mechanism behind the improved carrier confinement in our proposed graded QB structure, we have analyzed the net polarization charge density and electrostatic field in the active region. The electrostatic field in the active region can be estimated using the following Eqs 3–5.[27]

$$E_{\mathrm{QB}} \approx \frac{l_{\mathrm{QW}} \cdot \Delta P(z)}{l_{\mathrm{QW}} \cdot \varepsilon_{\mathrm{QB}} + l_{\mathrm{QB}} \cdot \varepsilon_{\mathrm{QW}}}, \tag{3}$$

$$E_{\mathrm{QB}} \cdot l_{\mathrm{QB}} = E_{\mathrm{QW}} \cdot l_{\mathrm{QW}}, \tag{4}$$

$$\Delta P(z) = \sigma^{pol}_{Sl_{\mathrm{interface}}} - \rho^{pol}_{B} \cdot z \tag{5}$$

where E_{QB} and E_{QW} denote the electrostatic field in the QB and QW, respectively. $\Delta P(z)$ represents the net polarization charge density; z is the position along the growth direction. $\varepsilon_{\mathrm{QB}}$ and $\varepsilon_{\mathrm{QW}}$ represent the dielectric constant of the QB and QW, respectively. l_{QW} and l_{QB} are the thickness of the QW and QB, respectively. $\sigma^{\mathrm{Pol}}_{\mathrm{Sl_{interface}}}$ is polarization-induced sheet charge density at the interface of QB and QW, and $\rho^{\mathrm{Pol}}_{\mathrm{B}}$ is polarization-induced bulk charge density in the QB. It is advantageous to have a lower electrostatic field in the QW region to confine the electrons and holes[15] effectively. From Eq 4, it is understood that reducing the value of E_{QB} can also reduce the value of $E_{QW.}$ Moreover, as shown in Eq 3, E_{QB} can be reduced by decreasing the value of $\Delta P(z)$. However, $\Delta P(z)$ is related to $\sigma^{\mathrm{Pol}}_{\mathrm{Sl_{interface}}}$ and $\rho^{\mathrm{Pol}}_{\mathrm{B}}$, as illustrated in Eq 5. Hence, these parameters are calculated for LED 2 and LED 3 as follows. The polarization induced sheet charge density at the QB/QW interface in $1/m^2$ is defined as a function of spontaneous, P_{SP} and piezoelectric polarizations, P_{PP},[28]

$$\sigma^{Pol}_{SI_{interface}} = \{P_{SP}(QB) - [P_{SP}(QW) + P_{PP}(QW)]\} \times 6.242 \times 10^{18}, \quad (6)$$

The P_{SP} and P_{PP} in C/m^2 can be written as[23]

$$P_{SP}(Al_xGa_{1-x}N) = -0.09x - 0.034(1-x) + 0.019x(1-x), \quad (7)$$

$$P_{PP}(Al_xGa_{1-x}N) = x \cdot P_{PP}(AlN) \cdot s + (1-x) \cdot P_{PP}(GaN) \cdot s \quad (8)$$

where $P_{PP}(AlN) = -1.808 \cdot s + 5.624 \cdot s^2$ for $s < 0$,
$P_{PP}(AlN) = -1.808 \cdot s + 7.888 \cdot s^2$ for $s > 0$,

$$P_{PP}(GaN) = -0.918 \cdot s + 9.541 \cdot s^2,$$

$$\text{Basal strain } (s) = \frac{QB_{\text{lattice constant}} - QW_{\text{lattice constant}}}{QW_{\text{lattice constant}}}$$

The values of the lattice constant can be found elsewhere.[28] Also, the polarization-induced bulk charge density(1/m^2) in the QB can be derived as follows. [29]

$$\rho^{Pol}_B = \frac{[P_{SP}(Al_yGa_{1-y}N) + P_{PP}(Al_yGa_{1-y}N)] - P_{SP}(Al_xGa_{1-x}N)}{z(y) - z(x)} \times 6.242 \times 10^{18} \quad (9)$$

Here, the QB is graded from $Al_xGa_{1-x}N$ to $Al_yGa_{1-y}N$, and $[z(y)\text{-}z(x)]$ is the grading distance. Finally, the calculated values of $\sigma^{Pol}_{SI_{interface}}$ and ρ^{Pol}_B for LED 2 and LED 3 are listed in Table III.

It is found that the $\sigma^{Pol}_{SI_{interface}}$ values are remarkably low in LED 3 compared to LED 2 due to the reduced lattice mismatch at the interfaces. In addition, the ρ^{Pol}_B values of the QBs are increased in LED 3 due to a compositionally graded Al profile. Altogether, in comparison with LED 2, the $\Delta P(z)$ values are reduced in graded QBs of LED 3. This leads to having a lower electrostatic field (E_{QB}) in all the QBs. Subsequently, it is also expected to achieve a lower electrostatic field (E_{Qw}) in the QWs of LED 3. The electrostatic field in the active regions of LED 2 and LED 3 are provided in Fig. 5. As predicted, multiple QWs of LED 3 exhibit lower electrostatic fields than LED 2, due to which carrier confinement is improved in LED 3.

Figure 6 illustrates the IQE, EL intensity, and L-I-V characteristics of all LEDs. The calculated maximum IQEs for LED 1, LED 2, and LED 3 are 35.69%, 29.45%, and 38.84%, respectively, as demonstrated in Fig. 6a. The IQE droop is ~94.7% under 0-60 mA current injection due to an increased electron leakage in LED 2. However, LED 3 exhibits a comparatively high IQE with an efficiency droop of only ~21.06%, while LED 1 has an efficiency droop of 53.68%, respectively. Such improvements in LED 3 are resulted from the improved radiative recombination and reduced electron leakage in the proposed structure. As a result, LED 3 displays dominant electroluminescence (EL) intensity compared to LED 1 and LED 2 at the emission wavelength of ~284 nm, as illustrated in Fig. 6b. Correspondingly, as illustrated in Fig. 6c, LED 3 shows a remarkable improvement in the output power ~12.12 mW at 60 mA current injection, which is enhanced by ~85.9% compared to the reference structure. Different calculated parameters related to IQE and output power of the three structures are provided in Table IV for comparison. As provided in Fig. 6d, the turn-on voltage of all three structures is nearly the same. However, it is inevitable that LED 3 exhibits a slightly higher operating bias voltage at 60 mA current injection than others due to the presence of graded QBs.

The output power of LED 3 is enormously increased with the input power supply at the same current injection level, as shown in Fig. 7a. We can also observe the different values of maximum operating input power supply in LEDs. This is mostly attributed to the different operation bias, as already described in Fig. 6d. The wall-plug efficiency (WPE) as a

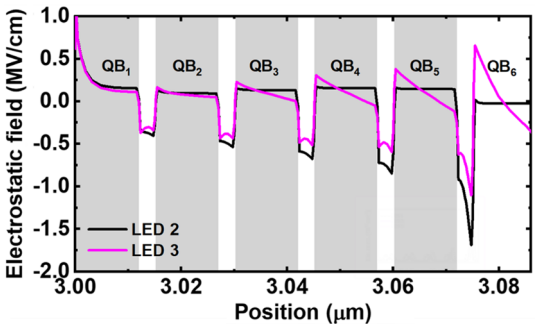

Fig. 5 The electrostatic field in the active region of LED 2 and LED 3.

Table III. Calculated σ_s^{Pol} at the QB/QW interface, (1/m^2) and ρ_B^{Pol} in the QBs, (1/m^3) of LED 2 and LED 3.

	σ_s^{Pol} QB2/QW2	ρ_B^{Pol} QB2	σ_s^{Pol} QB3/QW3	ρ_B^{Pol} QB3	σ_s^{Pol} QB4/QW4	ρ_B^{Pol} QB4	σ_s^{Pol} QB5/QW5	ρ_B^{Pol} QB5
LED 2	2.948×10^{16}	0	3.783×10^{16}	0	4.631×10^{16}	0	5.493×10^{16}	0
LED 3	2.672×10^{16}	2.348×10^{23}	2.672×10^{16}	9.468×10^{23}	2.672×10^{16}	$1.67`\times10^{24}$	2.672×10^{16}	2.404×10^{24}

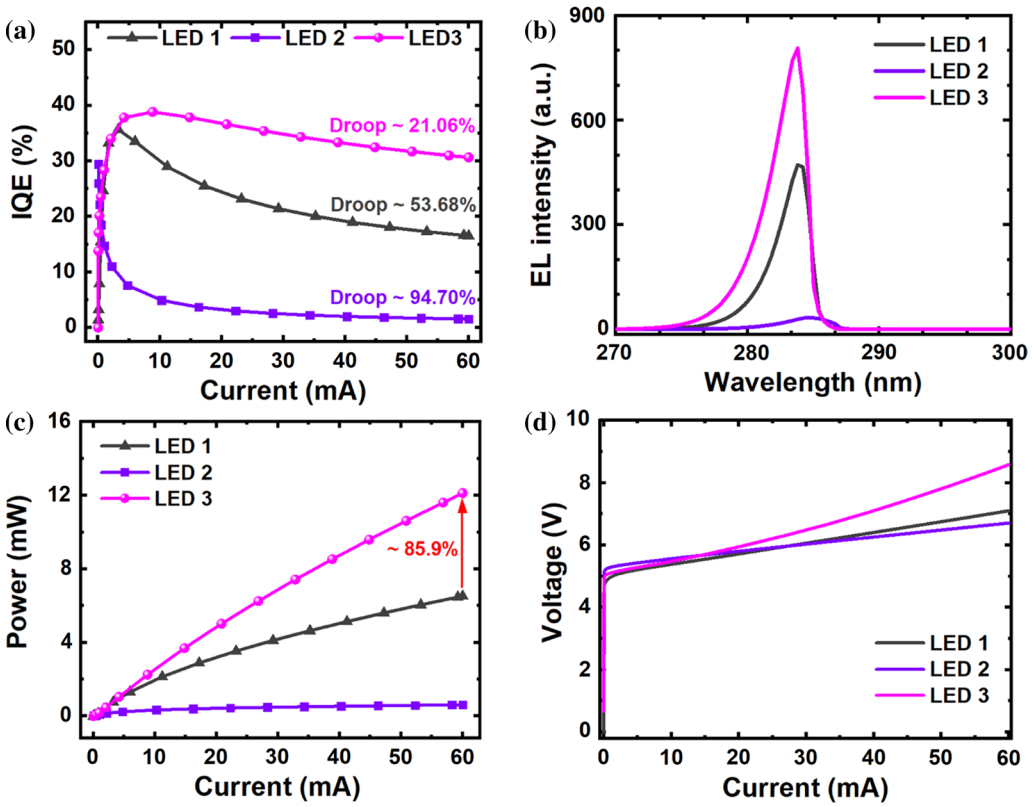

Fig. 6 Calculated (a) IQE, (b) EL intensity, (c) L-I, and (d) I-V characteristics of LED 1, LED 2, and LED 3.

Table IV. Comparison of IQE and output power of LED 1, LED 2, and LED 3.

	LED 1	LED 2	LED 3
Max. IQE (%)	35.69 at 3.26 mA	29.45 at 0.04 mA	38.84 at 8.82 mA
IQE (%) at 60 mA	16.53	1.56	30.66
IQE (%) droop	53.68	94.70	21.06
Power at 60 mA (mW)	6.52	0.61	12.12

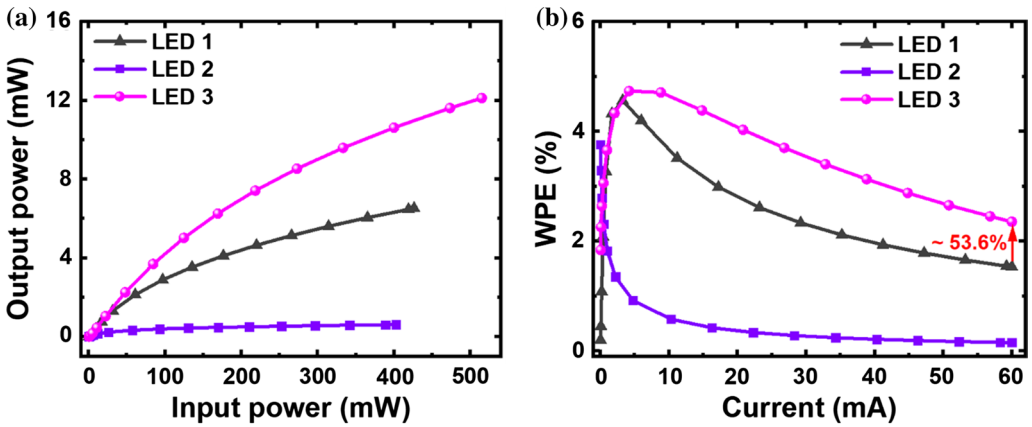

Fig. 7 Estimated (a) Output power as a function of input power, (b) WPE as a function of current injection of LED 1, LED 2, and LED 3.

function of current injection for all three LEDs is depicted in Fig. 6b. The superior WPE of the proposed structure results from the boosted output power, irrespective of having higher operating bias voltage values. Further, the WPE of LED 3 is found to be ~2.35% at 60 mA, which is improved by ~53.6% in comparison with the reference structure, LED 1.

Conclusion

In summary, we have reported and theoretically investigated the *p*-EBL-free AlGaN deep UV LEDs with the integration of linearly graded QBs at an emission wavelength of ~284 nm. The results show that incorporating the proposed QBs are advantageous for obtaining higher output optical power and WPE in AlGaN deep UV LEDs, mainly due to the engineered polarization in the active region. Another important benefit of the EBL-free structure from an epitaxial growth point of view is that we can eliminate the growth of p-heavily doped high-Al-composition AlGaN layers as EBLs for deep UV LEDs, which decreases the device resistance. Therefore, the reported structure has a great ability to produce high-performance UV LEDs for practical applications.

Conflict of interest The authors declare no conflict of interest.

Funding National Science Foundation (ECCS-1944312).

References

1. Y. Muramoto, M. Kimura, S. Nouda, Development and future of ultraviolet light-emitting diodes: UV-LED will replace the UV lamp. *Semiconduct. Sci. Technol*. 29, 084004 (2014).
2. M. Kneissl, T.-Y. Seong, J. Han, and H. Amano, The emergence and prospects of deep-ultraviolet light-emitting diode technologies. *Nat. Photonics* 13, 233 (2019).
3. R.T. Velpula, B. Jain, M.R. Philip, H.D. Nguyen, R. Wang, and H.P.T. Nguyen, Epitaxial growth and characterization of AlInN-based core-shell nanowire light emitting diodes operating in the ultraviolet spectrum. *Sci. Rep.* 10, 1 (2020).
4. R.T. Velpula, B. Jain, H.Q.T. Bui, T.T. Pham, H.-D. Nguyen, T.R. Lenka, and H.P.T. Nguyen, Numerical investigation on the device performance of electron blocking layer free AlInN nanowire deep ultraviolet light-emitting diodes. *Optical Materials Express* 10, 472 (2020).
5. B. Jain, R.T. Velpula, M. Tumuna, H.Q.T. Bui, J. Jude, T.T. Pham, A.V. Hoang, R. Wang, and H.P.T. Nguyen, Enhancing the light extraction efficiency of AlInN nanowire ultraviolet light-emitting diodes with photonic crystal structures. *Opt. Express* 28, 22908 (2020).
6. L. He, W. Zhao, K. Zhang, C. He, H. Wu, N. Liu, W. Song, Z. Chen, and S. Li, Performance enhancement of AlGaN-based 365 nm ultraviolet light-emitting diodes with a band-engineering last quantum barrier. *Opt. Lett.* 43, 515 (2018).
7. S. Sadaf, Y.-H. Ra, S. Zhao, T. Szkopek, and Z. Mi, Structural and electrical characterization of monolithic core–double shell n-GaN/Al/p-AlGaN nanowire heterostructures grown by molecular beam epitaxy. *Nanoscale* 11, 3888 (2019).
8. R.T. Velpula, B. Jain, H.Q.T. Bui, and H.P.T. Nguyen, Full-color III-nitride nanowire light-emitting diodes. *J. Adv. Eng. Comput.* 3, 551 (2019).
9. H. Hirayama, S. Fujikawa, N. Noguchi, J. Norimatsu, T. Takano, K. Tsubaki, and N. Kamata, 222–282 nm AlGaN and InAlGaN-based deep-UV LEDs fabricated on high-quality AlN on sapphire. *Phys. Status Solidi A* 206, 1176 (2009).
10. X. Ji, J. Yan, Y. Guo, L. Sun, T. Wei, Y. Zhang, J. Wang, F. Yang, and J. Li, Tailoring of energy band in electron-blocking structure enhancing the efficiency of AlGaN-based deep ultraviolet light-emitting diodes. *IEEE Photonics J.* 8, 1 (2016).
11. R.T. Velpula, B. Jain, H.Q.T. Bui, F.M. Shakiba, J. Jude, M. Tumuna, H.-D. Nguyen, T.R. Lenka, and H.P.T. Nguyen, Improving carrier transport in AlGaN deep-ultraviolet light-emitting diodes using a strip-in-a-barrier structure. *Appl. Opt.* 59, 5276 (2020).
12. B. Jain, R.T. Velpula, S. Velpula, H.-D. Nguyen, and H.P.T. Nguyen, Enhanced hole transport in AlGaN deep ultraviolet light-emitting diodes using a double-sided step graded superlattice electron blocking layer. *JOSA B* 37, 2564 (2020).
13. Y. Li, S. Chen, W. Tian, Z. Wu, Y. Fang, J. Dai, and C. Chen, Advantages of AlGaN-based 310-nm UV light-emitting diodes with Al content graded AlGaN electron blocking layers. *IEEE Photonics J.* 5, 8200309 (2013).
14. Z.-H. Zhang, S.-W.H. Chen, C. Chu, K. Tian, M. Fang, Y. Zhang, W. Bi, and H.-C. Kuo, Nearly efficiency-droop-free AlGaN-based ultraviolet light-emitting diodes with a specifically designed superlattice p-type electron blocking layer for high mg doping efficiency. *Nanoscale Res. Lett.* 13, 1 (2018).
15. B. So, J. Kim, T. Kwak, T. Kim, J. Lee, U. Choi, and O. Nam, Improved carrier injection of AlGaN-based deep ultraviolet light emitting diodes with graded superlattice electron blocking layers. *RSC Adv.* 8, 35528 (2018).
16. R.T. Velpula, B. Jain, S. Velpula, H.-D. Nguyen, and H.P.T. Nguyen, High-performance electron-blocking-layer-free deep ultraviolet light-emitting diodes implementing a strip-in-a-barrier structure. *Opt. Lett.* 45, 5125 (2020).
17. J. Yan, J. Wang, Y. Zhang, P. Cong, L. Sun, Y. Tian, C. Zhao, and J. Li, AlGaN-based deep-ultraviolet light-emitting diodes grown on high-quality AlN template using MOVPE. *J. Cryst. Growth* 414, 254 (2015).
18. Y. P. Varshni, Temperature dependence of the energy gap in semiconductors. *Physica* 34, 149 (1967).
19. C. Coughlan, S. Schulz, M. A. Caro, and E. P. O'Reilly, Band gap bowing and optical polarization switching in Al Ga N alloys. *Phys. Status Solidi B* 252, 879 (2015).
20. J. Yun, J.-I. Shim, and H. Hirayama, Analysis of efficiency droop in 280-nm AlGaN multiple-quantum-well light-emitting diodes based on carrier rate equation. *Appl. Phys. Express* 8, 022104 (2015).
21. H. Hirayama, Recent progress in AlGaN deep-UV LEDs. Light-Emitting Diode-An Outlook on the Empirical Features and Its Recent Technological Advancements (2018).
22. K. Nam, M. Nakarmi, J. Li, J. Lin, and H. Jiang, Mg acceptor level in AlN probed by deep ultraviolet photoluminescence. *Appl. Phys. Lett.* 83, 878 (2003).
23. V. Fiorentini, F. Bernardini, and O. Ambacher, Evidence for nonlinear macroscopic polarization in III–V nitride alloy heterostructures. *Appl. Phys. Lett.* 80, 1204 (2002).
24. S. Chuang, and C. Chang, k· p method for strained wurtzite semiconductors. *Phys. Rev. B* 54, 2491 (1996).
25. I. Vurgaftman and J. n. Meyer, "Band parameters for nitrogen-containing semiconductors. *J. Appl. Phys.* 94, 3675 (2003).
26. J. Piprek, "Efficiency droop in nitride-based light-emitting diodes. *Phys. Status Solidi A* 207, 2217 (2010).

27. Z.-H. Zhang, W. Liu, S.T. Tan, Z. Ju, Y. Ji, Z. Kyaw, X. Zhang, N. Hasanov, B. Zhu, and S. Lu, On the mechanisms of InGaN electron cooler in InGaN/GaN light-emitting diodes. *Opt. Express* 22, A779 (2014).
28. O. Ambacher, R. Dimitrov, M. Stutzmann, B. Foutz, M. Murphy, J. Smart, J. Shealy, N. Weimann, K. Chu, and M. Chumbes, Role of spontaneous and piezoelectric polarization induced effects in Group-III nitride based heterostructures and devices. *Phys. Status Solidi B* 216, 381 (1999).
29. D. Jena, S. Heikman, D. Green, D. Buttari, R. Coffie, H. Xing, S. Keller, S. DenBaars, J.S. Speck, and U.K. Mishra, Realization of wide electron slabs by polarization bulk doping in graded III–V nitride semiconductor alloys. *Appl. Phys. Lett.* 81, 4395 (2002).